Available online at www.sciencedirect.com

ScienceDirect

IFAC PapersOnline CONFERENCE PAPER ARCHIVE

IFAC PapersOnLine 51-28 (2018) 344–349

An Integrated Approach to Understanding the Impact of Network Resonances and Control on Dynamic Responses in VSC-HVdc Networks ⋆

Adedotun J. Agbemuko * **José Luis Domínguez-García** *
Oriol Gomis-Bellmunt **

* *Department of Electrical Power Systems*
Institut de Recerca en Energia de Catalunya (IREC)
Barcelona, Spain. (e-mail: aagbemuko@irec.cat, jldominguez@irec.cat).
** *Department of Electrical Engineering*
Universitat Politécnica de Catalunya
Barcelona, Spain. (e-mail: ogomis@upc.edu)

Abstract: An analysis of the impact of network and control in an interconnected system have been studied in this paper. Particularly, a simplified integrated approach is considered by modelling the entire network of devices and control in a multivariable feedback manner. In this way, the contribution of each device (via its impedance and/or control) and the network connection to responses observed can be understood in a tractable manner. The presented approach potentially provides a method that allows for manipulating observed responses via multivariable approaches. Results show the efficacy of the approach in providing a system perspective to dynamic responses by taking into account contributions. Analysis is carried out in frequency domain and validated with the physical model of the system built in Simscape™ Power Systems™ and control systems in MATLAB/Simulink®.

Keywords: VSC-HVdc Modelling, Dynamic performance, Multivariable control, Impedance-based modelling

1. INTRODUCTION

In a rapidly changing energy landscape buoyed by advances in power electronic devices, high voltage direct current (HVdc) systems are expected to play a central role in future transmission systems. The state-of-art of power electronic device for transmission is the voltage source converter (VSC) technology. HVdc systems based on this technology have been heralded as the backbone of future transmission networks. More so is the emergence of multi-terminal HVdc systems based on VSC technologies as a natural progression from the current point-to-point links to super-grids, Hertem and Ghandhari (2010).

Challenges of wide spread use of power electronics cannot be overemphasized, as established in the survey of Wang et al. (2013). An issue of interest in the academic and industrial community is the influence of often complex control structure on dynamic responses. The impact of the control system of these devices on system dynamics is well documented. The control system is usually a coupling agent, whilst the network acts as the facilitator. Poor controller design often result to undesirable interactions with other controllers. In a two terminal system, this may not necessarily be an issue. But in an interconnected multi-terminal system, with distinct devices from different manufacturers and a complex network structure, this would be a challenge. Therefore, understanding the influence of controls from a system perspective is key to realizing the vision for future power systems.

Motivated by the issues around power electronic converters as tightly controlled devices, the academic community has been applying several advanced methods for studies and analysis. A methodology rapidly gaining attention is the impedance-based modelling paradigm, see Sun (2011); Harnefors et al. (2007). This methodology has been widely applied at the device level for obtaining the equivalent model of converters connected to the grid, Cespedes and Sun (2014); Bing et al. (2009). More recently, the modelling paradigm is being increasingly applied to understand the sources of harmonic and resonance oscillations in wind power plants connected via power converters, Amin and Molinas (2017); Liu and Sun (2014); Xu et al. (2015), amongst other works.

However, the focus has usually being on the influence of one device on a unique network (such as wind farms), and at most two devices in the form of HVdc links. If the transition to RESs is to be plausible, then network would have to go beyond the influence of two devices to multitudes

⋆ This work was financially supported by the European Union's Horizon 2020 research and innovation programme under Marie-Sklodowska-Curie action INCITE – "Innovative controls for renewable source integration into smart energy systems", grant agreement No. 675318.

10.1016/j.ifacol.2018.11.726

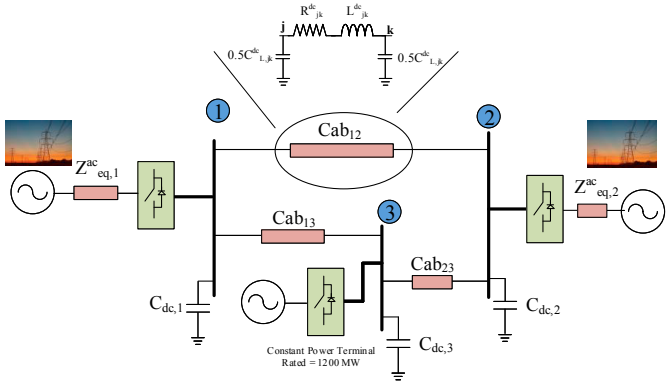

Fig. 1. Schematic diagram of a meshed VSC-HVdc system showing the main circuit impedances and Π circuit for each cable

of interconnected devices in constant interaction with one another. There is lack of literature on simplified methodologies, yet sufficient to understand the influence of control parameters and network on interconnected systems.

This paper employs the impedance-based modelling in a subsystem approach, to understand the influence of control and network in an interconnected system, with as many devices possible. A systematic approach is favoured in this paper as it becomes easy to integrate many different devices, control, and allow design of advanced controllers to mitigate interactions in a systematic manner.

2. SYSTEM DESCRIPTION AND IMPEDANCE MODELLING

Fig. 1 depicts the single line diagram overview of a multi-terminal dc grid with three interconnected terminals. As is typical in VSC-HVdc literature, at least one terminal is assigned to control the dc voltage, and others can operate in other modes. In this work, the converter at terminal 1 – VSC-1 plays this role. Since we are concerned mainly with the dc grid dynamics, the connected ac grids are duly simplified by an aggregate impedance (transformer and filter), with ac voltage assumed constant, i.e. there is no influence of ac voltage variations on the dc grid. This is a reasonable assumption for strong ac grids. However, ac current dynamics is essential to the operation of VSC-HVdc and is thus included.

2.1 The HVdc Grid

From the system depicted, several distinct subsystems can be identified viz. the converter and dc cables. Each converter with a distinct control mode is modelled once to allow for interoperability analysis and influence of different parameters. That is, each converter at each terminal with a distinct control system is modelled as a subsystem.

The dc cables are modelled by Π-equivalent models as shown in the inset of Fig. 1. The cable capacitances in the Π models on both ends are added to the respective dc bus capacitance as they are in parallel. Thus total capacitance at each terminal is given as (1),

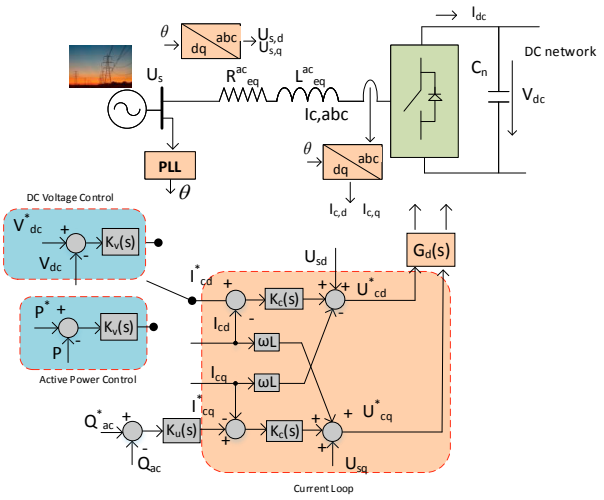

Fig. 2. Schematic diagram of the i$^{\text{th}}$ VSC Station and its control system based on vector current control

$$C_n = \sum C_{connected} = C_{dc,n} + 0.5 \sum_{\substack{j=1 \\ j \neq k}}^{n_c} C_{L,jk} \qquad (1)$$

where C_n is the total capacitance at terminal n, $C_{dc,n}$ models the dc terminal capacitance, $C_{L,jk}$ is the capacitance of the dc cable between terminals j and k, n_c is the total number of cables connected to terminal n. Sequel to this, each dc cable as a single subsystem is represented by the equivalent inductance and resistance in s-domain.

The converter is arguably the most complex subsystem in this study. Varying methodologies to represent the converter in studies are available in literature. At a system level, the VSC, regardless of its size or application is invariably a tightly controlled system. Therefore, the aim is to obtain an equivalent impedance, that combines the primitive impedance of the converter, and that of control. In this paper, we apply realistically simple averaged models appropriate for control and system level studies, Chaudhuri et al. (2014). Categorically, the method applied in this paper is done in the context of linear circuits and control theory for which superposition principle applies.

Fig. 2 depicts the schematic of the control systems of a HVdc station. The control system is implemented in the synchronous reference frame (SRF) typical of VSC HVdc, to allow compensators to control dc quantities, Yazdani and Iravani (2010). Other proposed controllers in literature, such as the droop control can be implemented as required. Additionally, each terminal is modelled initially as disconnected from the grid.

2.2 DQ Impedance Modelling of Converters

This section models the converter in the direct-quadrature (DQ) domain also known as the SRF, typical of HVdc control. Therefore, all derivations are in the framework of DQ domain.

2.3 DQ Modelling Current Controller

The analytical block diagram for the current control system is depicted in Fig. 2. The plant is modelled with its

admittance equivalent, $Y_{eq}^{ac}(s)$, of (2), since its inputs are the two voltages – grid voltage and converter ac voltage, and outputs the ac current. As depicted, the inner current controller interfaces the converter and physical system modelled by the filter and transformer impedance, given as

$$Z_{eq}^{ac}(s) = R_{eq}^{ac} + sL_{eq}^{ac} \tag{2}$$

where $R_{eq}^{ac} = R_{trfx} + R_f$, $L_{eq}^{ac} = L_{trfx} + L_f$ for transformer and filter respectively.

The closed-loop response of the current controller on the d-axis where the dc voltage lies, can be derived as

$$I_{cd}(s) = H_{cl}^{i}(s)I_{cd}^{*} - Y_{oc}^{dd}(s)U_{sd} \tag{3}$$

with

$$H_{cl}^{i}(s) = \frac{H_{ol}^{i}(s)}{1 + H_{ol}^{i}(s)}; \quad H_{ol}^{i}(s) = K_c(s)G_d(s)Y_s(s) \tag{4}$$

where H_{ol}^{i} is the open-loop gain, $K_c(s)$ is the current compensator based on proportional integral (PI) control and $G_d(s)$ models the converter modulation delay, and $Y_{oc}^{dd}(s)$ is the output admittance on d-axis (without q coupling term as reactive power reference is 0) is derived as

$$Y_{oc}^{dd}(s) = \frac{Y_{eq}^{ac}(s)}{1 + H_{ol}^{i}(s)} \tag{5}$$

Several methods are available in literature to find the controller $K_c(s)$ that meets specifications. The internal model control method, Harnefors and Nee (1998) is employed as it results to an ideal current controller. Parameters were tuned to obtain a time constant τ of 1.5 ms. Each VSC is equipped with the above current controller, whose reference is provided by outer-controllers (voltage, power, etc.). If the grid voltage is assumed constant (as is assumed for a strong grid connection), then, the U_{sd} term of (3) is neglected. This is equivalent to assuming an ideal current control. This holds if ac voltage is fairly constant. Therefore, (3) simplifies to

$$I_{cd}(s) = H_{cl}^{i}(s)I_{cd}^{*}. \tag{6}$$

2.4 DQ Impedance Modelling of Voltage Controlling VSC

This section derives the terminal dq impedance of the voltage controlled terminal. As depicted in Fig. 2, the direct voltage control loop provides the reference to the inner controller. The converter on the dc side is modelled based on current source philosophy. Thus, the dc voltage feedback and dynamics can be modelled with (7),

$$C_n \frac{dV_{dc}}{dt} = I_{dc} + \sum_{\substack{j=1 \\ j \neq k}}^{n_c} I_{jk} \tag{7}$$

where I_{jk} is the cable current. The closed-loop response can be derived as

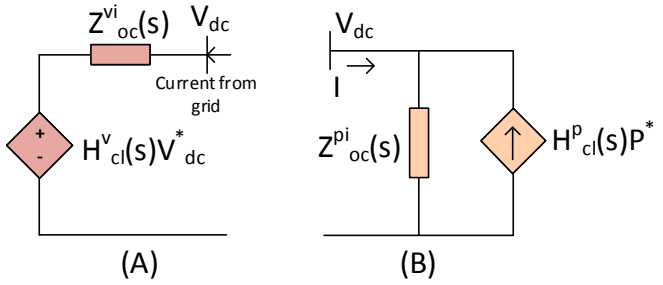

Fig. 3. Equivalent circuit representation of dc voltage and active power control terminals

$$V_{dc,i} = H_{cl}^{v}(s)V_{dc,i}^{*} + Z_{oc}^{v_i}(s)\sum_{\substack{j=1 \\ j \neq k}}^{n_c} I_{jk} \tag{8}$$

with

$$H_{cl}^{v}(s) = \frac{H_{ol}^{v}(s)}{1 + H_{ol}^{v}(s)}; \quad H_{ol}^{v}(s) = K_v(s)CH_{cl}^{i}(s)Z_{c_n} \tag{9}$$

where $H_{ol}^{v}(s)$ is the open-loop gain of the dc voltage controller, $K_v(s)$ is the compensator based on PI, C is a constant obtained from power balance equation between ac and dc grids (linearized conversion factor), and $Z_{c_n} = 1/sC_n$ is the impedance of the n^{th} terminal in s-domain. $Z_{oc}^{v_i}(s)$ is the dc terminal impedance of the voltage controlling converter without any adjoining network and can be derived as

$$Z_{oc}^{v_i}(s) = \frac{Z_{c_n}}{1 + H_{ol}^{v}(s)} \tag{10}$$

with $i = 1$ being the terminal controlling the voltage. Fig. 3A depicts the equivalent circuit representation of the closed-loop equation in (8).

2.5 DQ Impedance Modelling of Power Controlling VSC

This section models the active power controlling VSC. Power feedback is chosen to be from the dc bus (alternatively, the ac bus active power can be employed), where (11) holds as the power measurement

$$P_{m,i} = I_{dc,i}V_{dc,i} \tag{11}$$

for the i^{th} non dc voltage controlling terminal. Thus, $i = 2, 3$. Similar to the voltage controlling VSC, the active power loop provides reference to the inner current loop. The close-loop response can be derived as

$$P_{dc,i} = H_{cl}^{p}(s)P_{dc,i}^{*} - Z_{oc}^{p_i}(s)I_{dc,i}\sum_{\substack{j=1 \\ j \neq k}}^{n_c} I_{jk} \tag{12}$$

$$H_{cl}^{p}(s) = \frac{H_{ol}^{p}(s)}{1 + H_{ol}^{p}(s)} \tag{13}$$

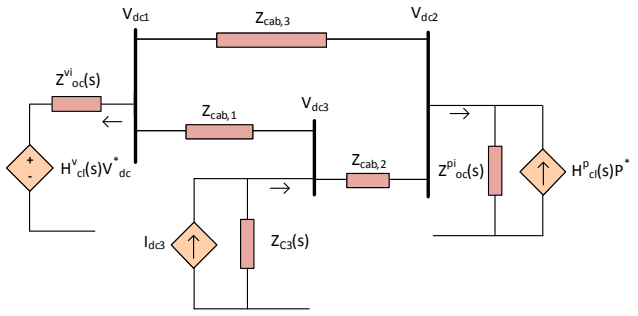

Fig. 4. Interconnected system with equivalent impedances

where $H^p_{ol}(s)$ is the open-loop gain, $Z^{p_i}_{oc}(s)$ is the dc terminal impedance of the power controlling VSC. $Z^{p_i}_{oc}(s)$ can be derived as

$$Z^{p_i}_{oc}(s) = \frac{Z_{c_n}}{1 + H^p_{ol}(s)}. \tag{14}$$

Fig. 3B depicts the equivalent circuit representation of the closed-loop response. The current source model can as well be transformed to a voltage source equivalent.

3. SYSTEM AGGREGATION

Each controlled terminal in Sections 2.4 and 2.5 were modelled as if disconnected from the grid. In order to carry out any analysis of the entire grid, connection must be made. This section aggregates the entire system based on the previously described procedures and Thévenin equivalent derivations, specifically, the nodal impedance method, first introduced in, Agbemuko et al. (2017).

3.1 Subsystem Interconnection

Fig. 4 depicts the system interconnection by equivalent impedances. As previously described, to maintain a uniform system aggregation, the current sources are transformed to equivalent voltage sources. However, as opposed to the voltage controlling terminal, the resulting equivalent voltage source is a current dependent voltage source. This is evident from the closed-loop response equation of the power loop.

The shown interconnected system can be compared to an ac equivalent with synchronous generation. Rewriting (8) and extending it to the entire network (keeping in mind the current dependency of the non-voltage controlling nodes) results to (15)

$$V^n_{dc} = V^{0n} + \Delta V^n \tag{15}$$

where, V^{0n} is control system response to input voltage reference, and ΔV^n is the disturbance response. Particularly, if the control system is guaranteed stable (in strict sense), at some point in time, the last term of (15) would cancel out. A similar conclusion can be made for linearization at a point. Thus, during disturbances, ΔV^n dictates the measured responses in V_{dc}. Note that the closed-loop control is explicitly included in ΔV^n through the sensitivity function $S(s)$. However, comparing the last term of the right-hand side of (8) and (15), ΔV^n is only dependent on local bus dynamics. This is not entirely true as it would be seen in the analysis section, the observed responses in an interconnected system are invariably coupled. That is, the network and control systems from other terminals contribute to the dynamics of a particular terminal.

3.2 Closed-loop Thévenin Derivation

To understand the contribution of each terminal to dynamic responses, we directly derive the closed-loop impedance matrix based on Thévenin's and superposition theorem. Interested readers are referred to The impedance model in Grainger and Stevenson Jr. (1994) for some insights on the physical interpretation of the impedance aggregation. The formulation of the nodal impedance matrix in (16) can be derived for the three terminal network.

$$\underbrace{\begin{bmatrix}\Delta V_1\\ \Delta V_2\\ \Delta V_3\end{bmatrix}}_{\Delta \mathbf{V}} = \underbrace{\begin{bmatrix}Z^{dc}_{11}(s) & Z^{dc}_{12}(s) & Z^{dc}_{13}(s)\\ Z^{dc}_{21}(s) & Z^{dc}_{22}(s) & Z^{dc}_{23}(s)\\ Z^{dc}_{31}(s) & Z^{dc}_{32}(s) & Z^{dc}_{33}(s)\end{bmatrix}}_{Z^{cl}_{bus}(s)} \underbrace{\begin{bmatrix}\Delta\Sigma I_{jk}\\ \Delta\Sigma I_{jk}\\ \Delta\Sigma I_{jk}\end{bmatrix}}_{\Delta \mathbf{I_{bus}}(i\neq j)} \tag{16}$$

$$Z^{cl}_{bus}(s) = \begin{bmatrix}Y^{dc}_{11}(s) & Y^{dc}_{12}(s) & Y^{dc}_{13}(s)\\ Y^{dc}_{21}(s) & Y^{dc}_{22}(s) & Y^{dc}_{23}(s)\\ Y^{dc}_{31}(s) & Y^{dc}_{32}(s) & Y^{dc}_{33}(s)\end{bmatrix}^{-1} \tag{17}$$

For the sake of brevity in this article, the nodal admittance matrix of Fig. 4 is inverted to obtain the nodal impedance matrix as it is easy to construct with less chance of errors. The availability of state-of-art of symbolic computing makes it possible to symbolically invert the nodal admittance matrix of any size. However, the mathematical rigor of deriving the impedance matrix is lost in the inversion procedure of the admittance equivalent. Thus, nodal admittance matrix does not offer any physical meaning as far as this work is concerned and is only utilized as it involves one mathematical step of inversion. The left hand side of (16) is the vector of voltage responses at each terminal for changes and/or disturbances in the entire system. In principle,

$$\Delta V \equiv \Delta V^n + \Delta V^{tr} \tag{18}$$

where ΔV^{tr} is the contribution transferred from other terminals. The $Z^{cl}_{bus}(s)$ is the dynamic transfer matrix of impedances. The principal diagonal elements are the dynamic Thévenin impedances, often referred to as the self-impedances for disturbances occurring at the respective terminal. Therefore they dictate the responses at their terminals for disturbances nearby (ac grid inclusive). The off-diagonal elements dictates the dynamic responses at a terminal for disturbances occurring at other terminals in the grid. The right-most vector is the changes in terminal currents due to disturbances in the grid. Each of the elements of the matrix is an input/output transfer function.

4. ANALYSIS

To provide some context, Fig. 5 depicts the frequency response sensitivity plot and time domain response of the terminal impedance, $Z^{v_i}_{oc}(s)$ from (8) for normalized system

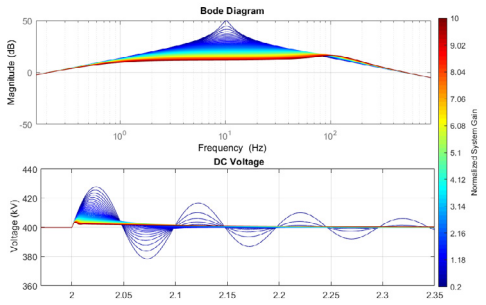

Fig. 5. Frequency response and time domain plot of terminal impedance at voltage controlling terminal

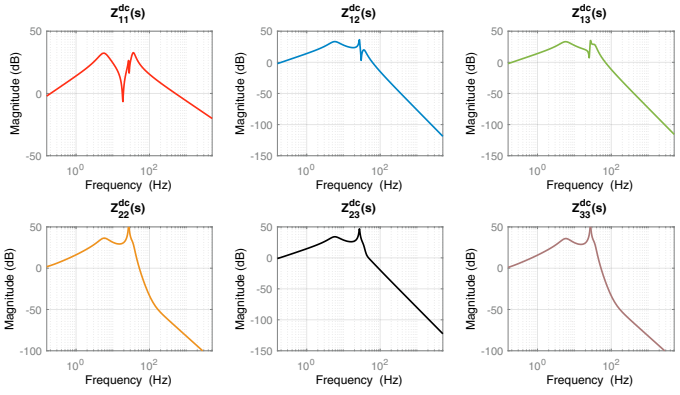

Fig. 6. Bode plot of closed-loop impedance transfer functions

gains and ideal current injection (that is, no adjoining network). Proportional gain is varied between 0.2-10 of the selected value based on second order tuning, that is, the selected value is 1. As gain is increased, control resonance around 10 Hz damps out and midpoint around a gain of 4, $Z_{oc}^{v_i}(s)$ has a flat response. As gain is increased further, around 7 a new resonance point start to appear at around 100 Hz. Physically, this is the point where the outer controller starts to interact with its inner controller. Beyond this point stability issues start developing. For value of 1, the time domain response is fairly smooth, adequate speed, overshoot within bounds. As would be observed in the sequel, this smooth response becomes degraded on interconnection.

Fig. 6 depicts the frequency response plot of each distinct elements of the closed-loop impedance matrix from (16) based on second order tuning procedures which only considers local dynamics. The obtained matrix is symmetric about the principal diagonal, as such there are only six distinct elements for a three terminal system. The nominal system parameters can be found in Tables 1 and 2. The phase plots are excluded as we are most interested in the magnitude and frequency.

At a first glance, the shape of the aggregated impedances (particularly $Z_{11}^{dc}(s)$) are different from that of Fig. 5 based only on the local dynamics. This underscores the influence of the network and other terminals in contributing to dynamic responses. For the case with local dynamics, only local control resonance can be observed. Elements pertaining to VSC-2 and VSC-3 are slightly similar by virtue of being both active power controlled terminals.

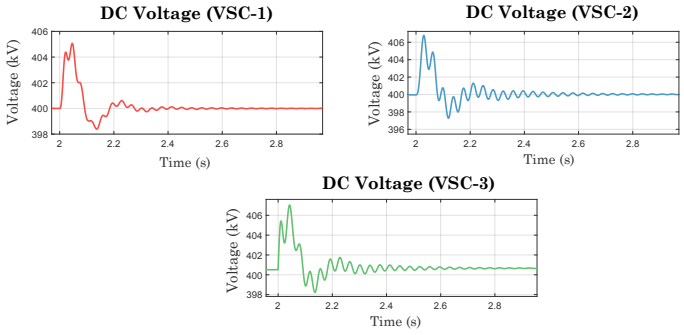

Fig. 7. Voltage responses for change in power flows in the dc grid

Ideally, all elements if the matrix should be as low (≈ 0) as available control system can allow, whilst maintaining strict stability. Diagonal elements can be reduced through robust tuning of local controllers for several expected disturbances, and off-diagonal elements by supplementary control. Generally, the resonance magnitude is lower in the interconnected network mainly due to the increased in capacitance afforded by cables. Additionally, the magnitude of the off-diagonal elements ($Z_{12}^{dc}(s)$, $Z_{13}^{dc}(s)$, $Z_{23}^{dc}(s)$) are as high as the diagonal elements which indicate strong interactions between terminals. Two resonant frequency are clear in off-diagonal elements, a slightly dominant point around 27-35 Hz mainly due to the influence of network at each terminal. Thus, interactions between terminals is mainly network dependent. As such, it may be sufficient to decouple the system by damping the network resonance. Diagonal elements for VSC-2 and VSC-3 show one dominant point which is the result of the small gains employed by power controllers. Diagonal element of VSC-1 show three resonant frequencies.

4.1 Evaluation and Simulations

To validate the efficacy of the described frequency domain analysis, the physical model of the network of Fig. 1 is built.

Fig. 7 depicts the voltage responses at each terminal for step changes in power flow in the grid. VSC-2 and VSC-3 both change their power references simultaneously. Thus, columns (2) and (3) of $Z_{bus,cl}(s)$ are of interest in this case. As can clearly be observed, the voltage response $V_{dc,1}$ at VSC-1 has three identifiable frequencies, VSC-2 and VSC-3 via the network, which matches with frequency domain responses. Frequency components of the voltage response of VSC-2 mainly consist of frequencies around 5.9 Hz and a dominant frequency component of 27 Hz. Whereas the frequency component of the voltage response of VSC-3 has components around 5.9 Hz and 35 Hz.

Fig. 8 depicts frequency responses for sensitivity with proportional gain of voltage controller. For lower values of the gain, off-diagonal element depict three resonant point, visible in the time domain responses. As gain is increased, some resonant frequencies damp out, leaving one dominant frequency also validated in time responses. At very high gain, the diagonal element for VSC-1 start to show a new resonance point already identified as the interaction point with the inner-loop of this terminal. Whereas for other

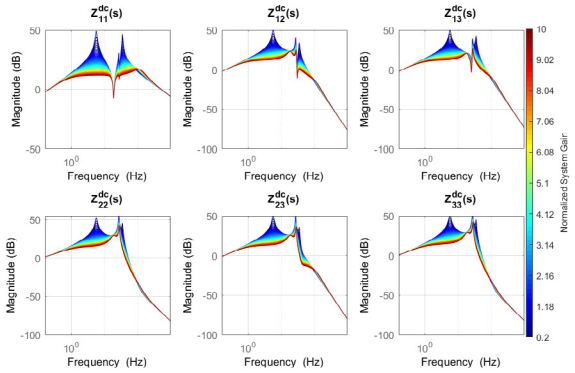

Fig. 8. Frequency responses for variation in proportional gain of voltage controller

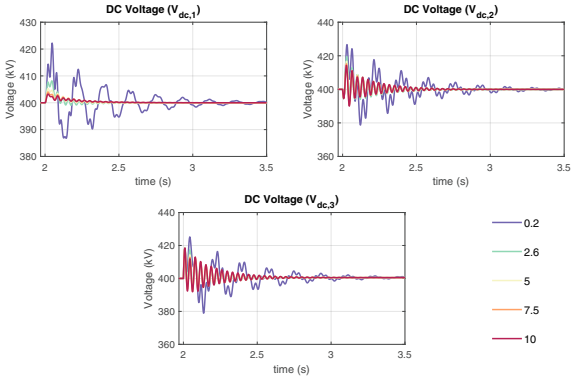

Fig. 9. Voltage responses for variation in proportional gain of voltage controller

Table 1. AC-DC Grid Parameters

Parameter	Value	Parameter	Value
Rated Power	1200 MW	R_{eq}^{ac}	0.006 pu
ac Voltage	220 kV (P-P)	L_{eq}^{ac}	0.327 pu
dc Voltage	400 kV (P-N)	C_{dc}	0.263 pu

Table 2. DC Cable Parameters

Parameter	Value	Parameter	Value
L_{dc}/km	2.615 mH	Cable 13	70 km
C_{dc}/km	0.1908μF	Cable 12	150 km
R_{dc}/km	0.011 Ω	Cable 23	100 km

elements, very high proportional gain of voltage controller do not make much difference.

5. CONCLUSIONS

In this paper, a simplified and integrated approach to modelling VSC-HVdc networks of arbitrary terminals and distinct devices have been presented. Simplifications were based on reasonable assumptions based on typical practice for studies such as this. Furthermore, equivalent circuits were obtained for each modelled subsystem in a manner that allows interconnection with the rest of the physical network. Network aggregation was subsequently carried out in a manner as to understand the differences between responses considering only local dynamics and the eventual response upon interconnection.

Results show the efficacy of the integrated approach. Ultimately, one noteworthy contribution is that there may be no need for computationally expensive time domain simulations to understand the influence of a connected device on a very large network.

REFERENCES

Agbemuko, A.J., Domınguez-Garcıa, J.L., Prieto-Araujo, E., and Gomis-Bellmunt, O. (2017). Harmonic stability and interactions in meshed vsc-hvdc dominated power systems. In *Proceedings of the 16th International Wind Integration Workshop*.

Amin, M. and Molinas, M. (2017). Understanding the origin of oscillatory phenomena observed between wind farms and hvdc systems. *IEEE Journal of Emerging and Selected Topics in Power Electronics*, 5(1), 378–392. doi: 10.1109/JESTPE.2016.2620378.

Bing, Z., Karimi, K.J., and Sun, J. (2009). Input impedance modeling and analysis of line-commutated rectifiers. *IEEE Transactions on Power Electronics*, 24(10), 2338–2346. doi:10.1109/TPEL.2009.2025333.

Cespedes, M. and Sun, J. (2014). Impedance modeling and analysis of grid-connected voltage-source converters. *IEEE Transactions on Power Electronics*, 29(3), 1254–1261. doi:10.1109/TPEL.2013.2262473.

Chaudhuri, N., Chaudhuri, B., Majumder, R., and Yazdani, A. (2014). *Multi-terminal direct-current grids: Modeling, analysis, and control*. John Wiley & Sons.

Grainger, J.J. and Stevenson Jr., W.D. (1994). *Power system analysis*. McGraw-Hill International Editions.

Harnefors, L., Bongiorno, M., and Lundberg, S. (2007). Input-admittance calculation and shaping for controlled voltage-source converters. *IEEE Transactions on Industrial Electronics*, 54(6), 3323–3334. doi: 10.1109/TIE.2007.904022.

Harnefors, L. and Nee, H.P. (1998). Model-based current control of ac machines using the internal model control method. *IEEE Transactions on Industry Applications*, 34(1), 133–141. doi:10.1109/28.658735.

Hertem, D.V. and Ghandhari, M. (2010). Multi-terminal VSC HVDC for the european supergrid: Obstacles. *Renewable and Sustainable Energy Reviews*, 14(9), 3156 – 3163. doi:http://dx.doi.org/10.1016/j.rser.2010.07.068.

Liu, H. and Sun, J. (2014). Voltage stability and control of offshore wind farms with ac collection and hvdc transmission. *IEEE Journal of Emerging and Selected Topics in Power Electronics*, 2(4), 1181–1189. doi: 10.1109/JESTPE.2014.2361290.

Sun, J. (2011). Impedance-based stability criterion for grid-connected inverters. *IEEE Transactions on Power Electronics*, 26(11), 3075–3078. doi: 10.1109/TPEL.2011.2136439.

Wang, H., Liserre, M., and Blaabjerg, F. (2013). Toward reliable power electronics: Challenges, design tools, and opportunities. *IEEE Industrial Electronics Magazine*, 7(2), 17–26. doi:10.1109/MIE.2013.2252958.

Xu, L., Fan, L., and Miao, Z. (2015). Dc impedance-model-based resonance analysis of a vsc-hvdc system. *IEEE Transactions on Power Delivery*, 30(3), 1221–1230. doi: 10.1109/TPWRD.2014.2367123.

Yazdani, A. and Iravani, R. (2010). *Voltage-sourced converters in power systems: modeling, control, and applications*. John Wiley & Sons.